

# Label-free wavelength and phase detection based SMS fiber immunosensors optimized with cladding etching

Yamile Cardona-Maya<sup>1\*</sup>, Abian B. Socorro<sup>2</sup>, Ignacio Del Villar<sup>2</sup>, José Luis Cruz<sup>3</sup>, Jesus M. Corres<sup>2</sup>, Juan F. Botero-Cadavid<sup>1</sup>

<sup>1</sup> School of Physics, Universidad Nacional de Colombia – Medellín Campus, Colombia

<sup>2</sup> Institute of Smart Cities (ISC), Public University of Navarra, 31006 Pamplona, Spain

<sup>3</sup> Department of Applied Physics and Electromagnetism, University of Valencia, Burjassot 46100, Spain

Corresponding author: [ycardon@unal.edu.co](mailto:ycardon@unal.edu.co)

## ABSTRACT

The performance of E-SMS (Etched Singlemode-Multimode-Singlemode) optical fiber structures as immunosensors has been assessed by the implementation of antibody/antigen immunoassays. Through this procedure it has been proven that E-SMS structures are effective and suitable optical platforms for label-free biosensing.

Using the phase shift and tracking the wavelength response it was found that the fabricated E-SMS devices exhibited limits of detection (LOD) down up to concentrations of 0.2 mg/L of antigens in solution. This was achieved by coating the E-SMS with an antibody-based biolayer (goat IgG) that is able to determine the presence of anti-goat IgG antigen. Both a wavelength detection and a fast Fourier transform (FFT) analysis technique were used to perform this analysis. The FFT method showed similar results to those observed with the most traditional wavelength analysis, but with the advantage of a simpler detection system that makes unnecessary the use of sophisticated optical interrogators.

## INTRODUCTION

The development of real-time detection devices, especially label-free biosensors with high selectivity for the recognition of low concentrations of analytes with rapid response, is an innovative field in applied research and healthcare diagnostics [1], [2].

Optical biosensors have proved to be a powerful solution for the detection and analysis in biomedical research applications [3]. Commonly, there are two detection protocols that can be implemented in optical biosensing: labelled detection and label-free detection. Labelled detection involves the use of a label, i.e. the optical signal is generated by a colorimetric, fluorescent, or luminescent method. Labelled detection techniques can be extraordinarily sensitive, exhibiting detection limits even down to a single molecule [4], [5], but it often involves tedious labelling processes that may also interfere with the function of the biomolecules [1]. On the other hand, in label-free detection molecules are not labeled or modified, and quantitative and kinetic measurement of molecular interaction can be achieved [1].

When an optical transducer is used as a biosensor, the working principle involved in the label-free detection is the modulation of the optical signal induced by the change of the refractive index (RI) at the biolayer. A biolayer is a coating where the biorecognition molecules are immobilized and the interaction with the biomolecule under investigation occurs. Generally, the modification of the optical signal is derived from the interaction of the evanescent wave with the outermost layer [6].

Up to now, multiple fiber optic structures have been studied for label-free detection biosensors, including those based on surface plasmon resonance [7], [8], photonic crystal [9], long period gratings [6], [10], and interferometers [11], [12]. The need for recognition of low concentrations of analytes, which involves small changes of RI, makes it necessary to use very sensitive refractometers for this purpose. This detection task can be achieved through fiber optic immunosensors, which are refractometric sensors with a biolayer. In this way, target molecules are detected when they interact with the biolayer.

Among the different optical structures that can be used, a simple waveguide based on interferometry has been used in this article. An SMS (single mode–multimode–single mode) configuration consists of two single mode fibers (SMFs) which are spliced to the ends of a section of a multimode coreless fiber (MMF). When the light propagating along the input SMF enters the MMF section, multiple eigenmodes of the MMF are excited and thus, interference among different modes occurs during the propagation along this MMF section. This is also known as multimode interference (MMI) [13]. Through the reduction of the diameter in the MMF section by chemical etching of the waveguide material, the evanescent field of the guided light in this section further penetrates into the surrounding medium,

therefore increasing its sensitivity [14], [15]. The result is an SMS with etching, hereinafter called E-SMS (Etched-SMS).

On the basis that the sensitivity to refractive index is inversely proportional to the SMS diameter [16], the feasibility of E-SMS structures as biosensors has been proven recently [17]. In that work two SMS structures, one without etching (125- $\mu\text{m}$  diameter) and one with etching (15- $\mu\text{m}$  diameter), were analyzed. The etched structure was able to detect the bound of anti-IgGs to the IgG-based biolayer, whereas the unetched structure could not perform this detection due to its lack of sensitivity. It is evident that the sensitivity of a biolayer is not always directly related to the bulk refractive index sensitivity and a thorough analysis could be done on the influence of the diameter on the sensitivity to the creation of a biolayer. However, considering the results of [17], where the sensitivity was improved as the diameter was reduced, in the current work we used a structure with a 25- $\mu\text{m}$  diameter, which allows a good sensitivity to be achieved while still being not too brittle that it could be handled properly. In spite of this approach, the quality of the interference spectrum achieved was not optimum and it was thought that the results could be improved by holding the fiber structure straight. In the present contribution, an optimum interference spectrum is defined when the interference bands are periodically spaced, which in turn simplifies the tracking of the interferometric bands. This allows the use of a Fast Fourier Transform (FFT) analysis, as will be developed later in this work.

In addition to the improvement of the spectral conditions for the tested E-SMS, a flow cell has been designed and used to guarantee a temperature control during the immobilization and detection of the target molecules. With these upgrades, it has been possible to attain a limit of detection (LOD) of 0.2 mg/L, whereas the lowest antigen concentration detected was 1 mg/L. This improves by a factor of 41.8 the lowest value detected with the same structure in reference [17], which was only of 41.8 mg/L. This proves that the E-SMS structure is an alternative to other devices, but with an easier and more cost-effective fabrication.

## **METHODS AND MATERIALS**

### **1. Etching of the SMS fiber structure**

Coreless MMF segments from POFC Inc. (Taiwan) and standard SMF pigtailed from Telnet Redes Inteligentes Inc. (Zaragoza, Spain) were used in this research. The SMS structures were built by splicing standard SMF pigtailed on each end of 14-mm segments of coreless MMF, as shown in Fig. 1(a), using a FITELE S178A V2 Fusion splicer machine was used for all splices in automatic mode. These structures were etched using an aqueous solution of hydrofluoric acid (HF) at a 40% concentration until the diameter of the structures were approximately 25  $\mu\text{m}$  (see Fig. 1(b)). This etching stage took 60 minutes. The effect of the etching was studied both numerically and experimentally.

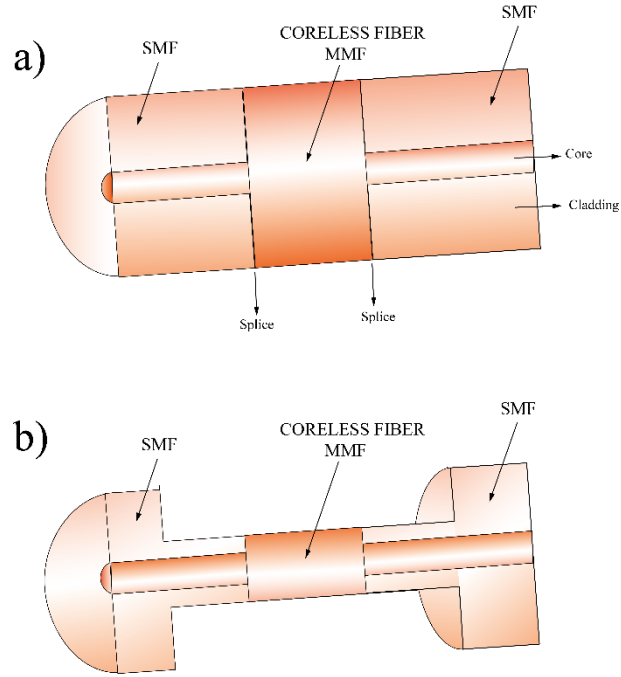


Fig. 1 (a) 14-mm segment of coreless MMF spliced on each end to standard SMF forming an SMS structure, (b) E-SMS structure after the HF etching.

The numerical analysis of this structure was performed using FIMMWAVE<sup>®</sup>. The propagation was analyzed through FIMMPROP, an integrated module of FIMMWAVE<sup>®</sup>. The Finite difference method (FDM) was used for the SMF and MMF sections, since it is the most accurate method available for cylindrical waveguides. In the SMF sections, only the fundamental mode was analyzed, whereas for the MMF section 30 modes were analyzed; thus, convergence was achieved in the results. The refractive index of the optical fiber cladding, made of fused silica, was estimated by using the Sellmeier equation:

$$n^2(\omega) = 1 + \sum_{j=1}^m \frac{B_j \omega_j^2}{\omega_j^2 - \omega^2} \quad (1)$$

with parameters [18]:  $B_1=0.691663$ ,  $B_2=0.4079426$ ,  $B_3=0.8974794$ ,  $\lambda_1=0.0684043 \mu\text{m}$ ,  $\lambda_2=0.1162414$ , and  $\lambda_3=9.896161$ , where  $\lambda_j=2\pi c/\omega_j$  and  $c$  is the speed of light in vacuum. The optical fiber core refractive index for the simulations was obtained according to the specifications from the fiber manufacturer through increasing the refractive index of the cladding 0.36%.

The etching stage was carried out by using the following procedure. The SMS structure was located in a plastic container with small lateral slits to hold it in place and the cavity of the container was filled with the HF solution. The liquid did not leak through the side slits due

to the surface tension of the HF. Simultaneously, light from a broadband light source (Agilent 83437A) was launched through the SMS structure and an Optical Spectrum Analyzer (Agilent 86140A) recorded the transmission spectrum during the etching stage. This etching lasted until the diameter of the fiber was reduced to 25  $\mu\text{m}$ , after an elapsed time of 60 minutes. Fig. 2 illustrates the experimental setup employed during the etching stage. A more complete description and results of this procedure can be found in [19].

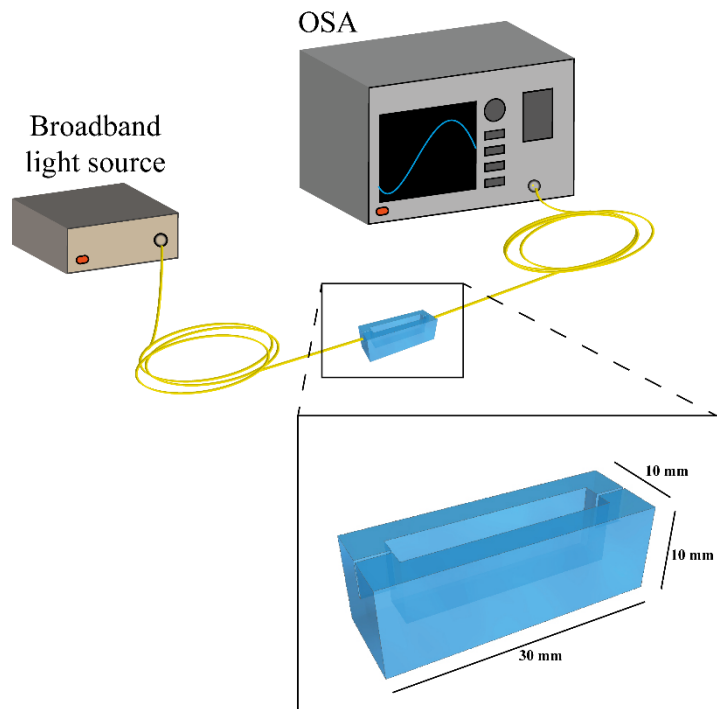


Fig. 2 Experimental Setup for etching the SMS structure

## 2. Fluidic system

Taking the flow cell proposed by Trono *et al.* [20] as a model, a fluidic system was designed to control temperature while at the same time small amounts of the reagents flowed parallel to the sensor, thus increasing the effective area of the sensor in contact with these reagents. The fluidic system consisted of a flow cell that kept the optical fiber firmly straight, a peristaltic pump controlled by a stepper motor, and a temperature-compensated control.

The flow cell was made of two main parts. The upper part was a 10-mm thick PMMA piece, whereas the lower part was a 10-mm thick aluminum piece placed in thermal contact with two Peltier cells (see Fig. 3). The whole system was mounted on a cooler (heat sink and fan). The flow cell was 80-mm length, 23-mm width and 10-mm height. The flow channel was a

rectangular section groove incised in the aluminum piece, running along the length of the flow cell with a 50- $\mu$ L volume. The PMMA piece had two holes aligned with the flow channel serving as inlet and outlet ports for the tested fluid.

The entire E-SMS sensor with its outer acrylate jacket was fastened to the groove ends using UV optical flexible adhesive (Norland 65). After the UV polymerization, a complete sealing of the flow cell is ensured by using a Parafilm<sup>®</sup> membrane sandwiched between the upper and lower pieces.

One of the objectives of this study was to determine the role of temperature control in the bioassays. The temperature stabilization of the flow cell was achieved by a closed-loop control. An NTC thermistor (926-1108-ND, Digi-key) inserted into the aluminum piece in the vicinity of the flow channel acted as a feedback element for the Peltier elements, which in turn were driven by a temperature controller (739-TC-14-PR-59, Laird Technologies / Thermal Solutions). The temperature of the flow cell was measured by another NTC thermistor placed inside the PMMA piece in the vicinity of the flow channel. The temperature data acquisition was performed using a PC via the RS-232 serial interface with two different resolution situations that will be described further on in this paper.

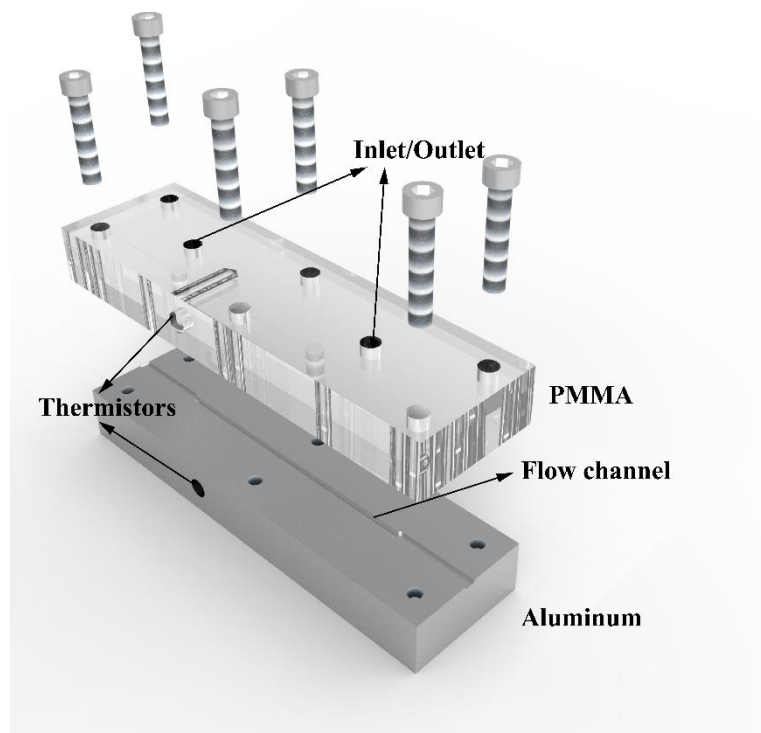


*Fig. 3 Flow cell composed by two parts: a PMMA piece (upper) and an aluminum piece (lower).*

### 3. Chemical treatment of E-SMS and bioassay protocol

Every biosensor is composed of three well-differentiated parts: the substrate, the biolayer, and the immobilization interface. The substrate in this proposed biosensor is the E-SMS, where the optical transduction process occurs. The biolayer is in charge of detecting the target molecules based on the corresponding bioreactions. According to the target biomolecule, biosensors can be classified as enzyme/protein-based sensors, immunosensors, cell/tissue sensors, aptasensors (sensors based on DNA chains), or even microorganisms-based sensors. In this work, an antigen/antibody interaction was studied, leading the path to developing an immunosensor. Finally, the immobilization interface provides the biolayer attachment to the substrate. In the last decades a wide variety of immobilization techniques have been developed and have been used for biosensing applications [21].

For this research, a coating or biolayer, was deposited onto the surfaces of two E-SMS, hereinafter called E-SMS 1 and E-SMS 2, to detect the presence of anti-goat IgGs (Sigma Aldrich G4018). The biolayer was composed of a film of IgGs from goat serum (Sigma Aldrich I9140) with a concentration of 11.4 mg/mL. Fig. 4a presents a schematic of the functionalization procedure steps executed. First, the E-SMS surfaces were functionalized by immersion in a solution of Eudragit L100 (Evonik) copolymer using ethanol as solvent. The polymeric deposition provides carboxylic functional groups ( $\text{—COOH}$ ) to the surfaces, useful for IgGs immobilization. Once the E-SMS was functionalized, it was placed into the flow cell and the following steps were performed to fabricate the biolayer: 1) activation of  $\text{—COOH}$  groups by means of EDC (Thermo Fisher 22980) and NHS (Thermo Fisher 24500); 2) covalent immobilization of the antigen on the E-SMS surface by pumping a solution of IgG in PBS; and 3) surface passivation with 1% BSA in PBS in order to achieve surface passivation. The deposition procedure, solution concentrations, and times involved were followed as presented previously reported in reference [6]. Fig. 4b presents the final scheme of the proposed biosensor based on an E-SMS.

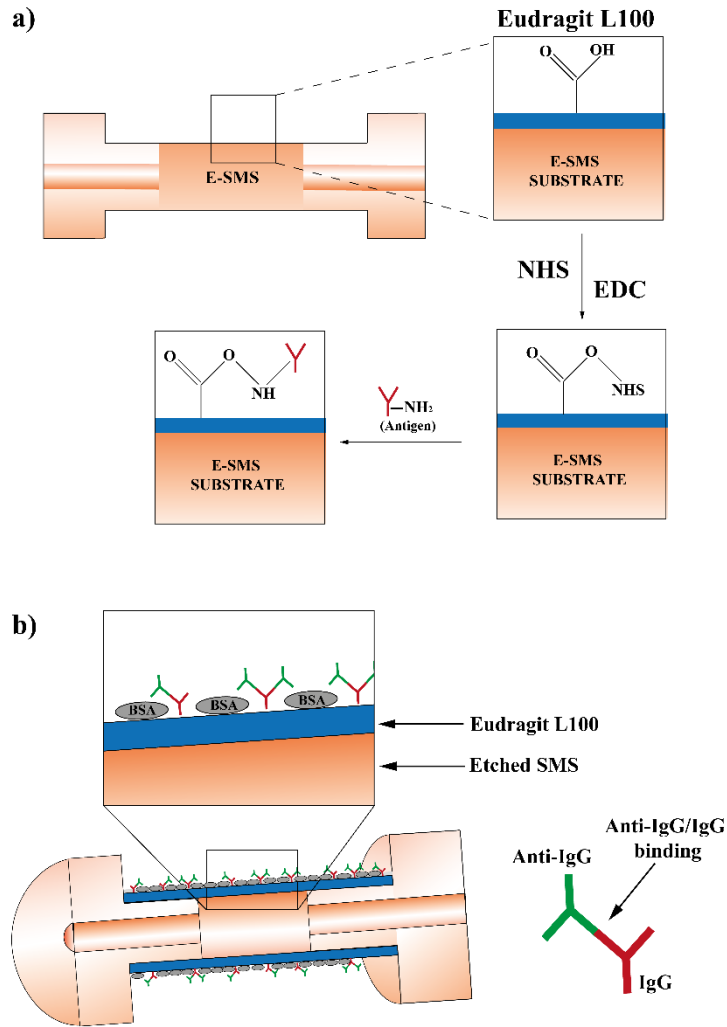


Fig. 4. a) Schematic of the functionalization procedure steps executed, b) Scheme of the proposed biosensor based on an E-SMS. After the deposition of the biolayer, the interaction between the coupled cladding mode and the surrounding environment causes an RI change within the layer.

A crucial aspect to control throughout the whole process was the influence of the temperature on the results. In order to analyze this, the temperature during the bioassay with the E-SMS 1 was set to fluctuate with an error of  $0.5\text{ }^{\circ}\text{C}$ , but in the case of the E-SMS 2, an improvement on the parameters of the temperature controller was carried out and an error of approximately  $0.01\text{ }^{\circ}\text{C}$  was attained. The room temperature and flow cell temperature were kept at  $25\text{ }^{\circ}\text{C}$  and  $30\text{ }^{\circ}\text{C}$ , respectively. For all the experiments a  $250\text{ }\mu\text{L}/\text{min}$  flow rate was used.

Once the biolayer was deposited, several solutions in PBS with increasing concentrations of anti-goat IgG were pumped into the flow cell. A washing stage of the flow cell using PBS buffer (phosphate-buffered saline, pH 7.4) between each new anti-goat IgG concentration was necessary to determine both wavelength and phase shift due to new anti-goat IgG binding to the biolayer.

The variation of the previous parameters for an attenuation band of the E-SMS as a function of the anti-goat IgG concentration, could be fit through a logistic curve that described the sigmoidal response of a biosensor [22]. In this research, the Hill equation was chosen to characterize this sigmoidal behavior [23], [24].

From the calibration curve, it was possible to determine parameters such as: the dynamic signal range (DSR), the working range (WR), and the limit of detection (LOD) of the biosensor. The DSR was the difference between the two horizontal asymptotes of the sigmoidal curve. The WR was calculated by considering the antigen concentration range between 10% and 90% of the DSR [25]; and finally, LOD can be obtained from the calibration curve through the inverse of the fitting Hill function evaluated in a well-defined point: the mean value of the blank sample ( $\bar{y}_{\text{blank}}$ ) plus three times the maximum standard deviation ( $\sigma_{\text{max}}$ ) obtained among all the experimental points. This can be expressed by the following equation:

$$X_{\text{LOD}} = f^{-1}(\bar{y}_{\text{blank}} + 3\sigma_{\text{max}}) \quad (1)$$

This approach, proposed by Chiavaioli et al [26], represents a valuable option for evaluating the LOD within a certain degree of reliability and repeatability, e.g. when the bioprobes can not be repeated with the same device, as the case here exposed.

When the sensor is exposed to each solution, both wavelength and phase evolve in an exponential manner. In order to report a magnitude for each new concentration, an average of the signal values during the PBS washing step following the immersion at that particular concentration was taken. This approach was taken since it allowed the response changes due to the anti-goat IgG effectively bound to the goat IgG of the bilayer to be measured. The experimental datum at 0 mg/L of anti-goat IgG concentration was the value taken in PBS before exposing the biosensor to any anti-goat IgG concentration.

In order to test the sensor from the baseline for each antiIgG concentration it would be needed to use a new sensor each time. This would be inefficient in terms of time and could compromise the repeatability of the measurements. Consequently, a good idea could be to regenerate the sensor (i.e. to suppress the bounds between IgGs and antiIgGs without destroying the Eudragit layer). We are working on how to apply a solution that permits to regenerate the sensor and to reuse it multiple times, which should permit to test the sensor from the base line for each antiIgG concentration.

#### **4. Characterization and optical setup**

Generally, interferometric sensors are characterized by tracking the wavelength shift of an attenuation band by using an optical spectrum analyzer or, alternatively, by measuring the intensity variations at a fixed wavelength using a power meter. Despite the fact that the fast Fourier transform (FFT) analysis provides useful and clear information to be used in sensing applications, it is not a commonly used technique. FFT analysis allows the phase of the

optical spectrum to be obtained, and simplifies the detection setup since optical interrogators can be used instead of more expensive optical spectrum analyzers [27], [28].

As mentioned in the introduction of this work, an optimum spectrum obtained from an E-SMS shows a periodic response of the interference peaks. This periodicity enables the achievement of a sharp peak corresponding to the fundamental frequency after performing the FFT analysis. Fig. 5 presents the contrast between the magnitude of the fast Fourier transform before and after etching. Therefore, it is possible to obtain a phase sensitive device by tracking the phase of this fundamental frequency as a function of the parameter to detect. In order to prove the feasibility of this method for the developed immunosensor, several bioassays were performed monitoring both the phase and the wavelength shifts for an attenuation band. A MATLAB<sup>®</sup> script was then implemented to obtain the real-time phase of the fundamental frequency along with the optical spectrum response of the sensor.

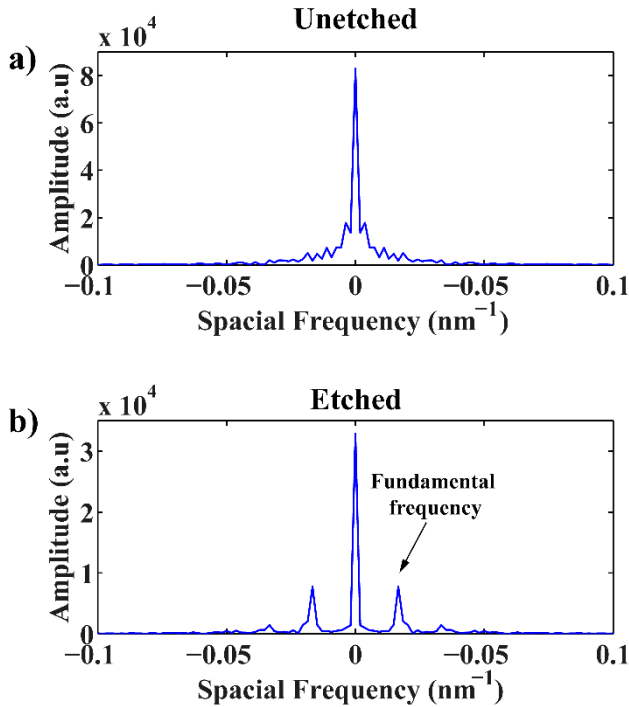


Fig. 5 Theoretical amplitude of the fast Fourier transform (a) SMS with 125  $\mu\text{m}$  diameter and (b) E-SMS with 25  $\mu\text{m}$  of diameter.

Keeping this in mind, two optical fiber refractometers, E-SMS 1 and E-SMS 2, were fabricated as described in section 1 and then used to perform two bioassays. In each bioassay, the corresponding E-SMS was placed inside the flow cell system. The optical setup employed to measure the light spectrum transmitted through the E-SMS sensor consisted of a broadband light source illuminating the E-SMS and an OSA recording the transmission spectrum during all stages. The OSA was connected to a PC performing the calculation of the evolution of the phase and wavelength shifts in real-time for an attenuation band in the transmitted spectrum at all stages along the bioassay.

Fig. 6 illustrates the schematic diagram of the proposed measuring setup. The E-SMS inside the flow cell was exposed to the solution at the adequate concentration stored in an Eppendorf container. Each time a new solution needed to be injected into the system, the hose tip that imbibed the fluid was removed from the container with the old solution, and then immersed in a new Eppendorf container with either the solution at a new concentration or the PBS solution for the washing step. An alternative method to reduce the amount of liquid used in the flow cell, could be not to feedback the liquid going out of the flow cell. In that case, it would be necessary to soak the liquid from the Eppendorf at a flow rate that avoids consuming it completely.

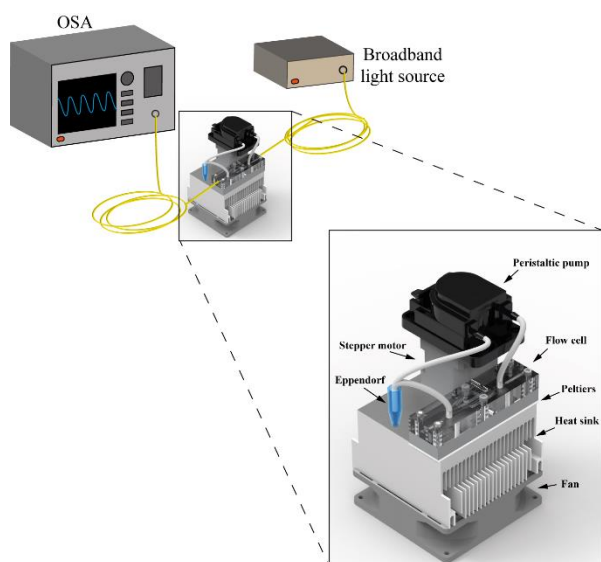


Fig. 6 Working setup

## 5. Temperature cross-sensitivity, repeatability, and selectivity

In order to determine the temperature cross-sensitivity of the E-SMS, the control temperature was set to 30 °C and the spectra was recorded during 13 minutes after reaching this set point. After this time, the control was set to 40 °C and kept at this constant temperature for 5 minutes, then lowered back to 30 °C and recorded for 15 minutes after reaching the lower set point, and finally set back at 40 °C for and recorded for another 5 minutes once it was reached this upper set point. The real-time wavelength shift was recorded and processed along with the entire procedure of temperature variation.

Regarding to the repeatability of the bioassays, we performed five bioassays with different anti-IgG concentration values to test the ability of the sensor to follow a curve that does not depend in a great manner on the concentrations applied. The E-SMS biosensors used were manufactured with the same procedure.

Concerning with establishing the selectivity of the bioprobes, cross-sensitivity to other biomolecules of the E-SMS biosensor has already been studied in [16]. Anti-gliadin antibodies (AGAs) were exposed to the biosensor in order to determine the selectivity. In this research, an additional specificity test was performed. Here an additional biomolecule, C-reactive protein (CRP), was chosen to confirm the selectivity of the device. Several solutions in PBS with increasing concentrations of anti-goat IgG and CRP were pumped into the flow cell separately where one of the E-SMS structures coated with the IgG-based biolayer was placed. The temperature was set to 30 °C, and it was controlled with an error of 0.01°C. A washing stage of the flow cell using PBS buffer between each new concentration was necessary to determine both wavelength and phase shift due to the respective binding.

## **RESULTS**

### **1. Optimization of the E-SMS structure**

Fig. 7 (a) and (b) show the experimental and numerical transmission spectra for both, etched and unetched fibers.

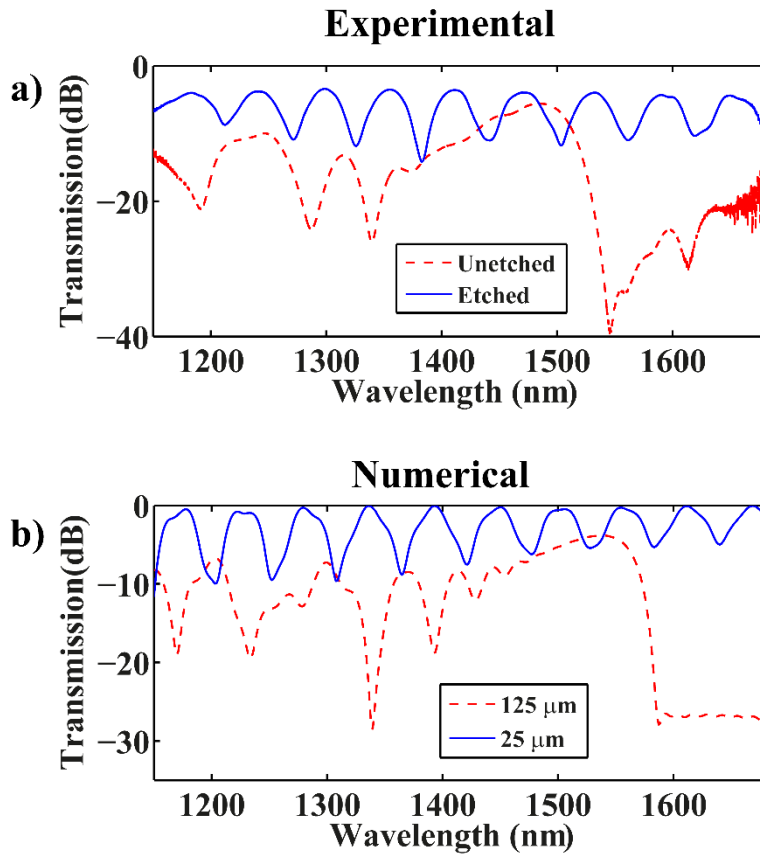


Fig. 7 Comparison between the spectra of unetched and etched fibers: (a) experimental; (b) Numerical

In order to observe the wavelength shift, the E-SMS structure was immersed in various solutions of glycerol in water at different concentrations [29], [30]. The sensitivity curve was obtained after tracking the spectral changes of the nearest attenuation band to 1310 nm within the extended telecommunications window, where common optical equipment operates. This characterization was performed both experimentally and numerically before depositing the bilayer (see the experimental points and the numerical red line in Fig. 8). The numerical results were obtained with FIMMWAVE.

The sensitivities to changes in the refractive index for a range of indices from 1.32 to 1.41 were approximately 740 nm/RIU for both studied cases. However, it is well known that the response sensitivity exhibits a non-linear behavior increasing at high RIs, as shown in Fig. 8. In the case of immunosensing applications, the most suitable values of RIs were within the range of 1.32-1.35, close to that of water and other physiological fluids. In consequence, for the studied cases, the sensitivities obtained both experimentally and numerically in this range of RIs were 280 nm/RIU and 270 nm/RIU, respectively. These sensitivities were calculated for the experimental points as a linear regression with a maximum standard deviation of 0.1 nm and a correlation coefficient of 0.97.

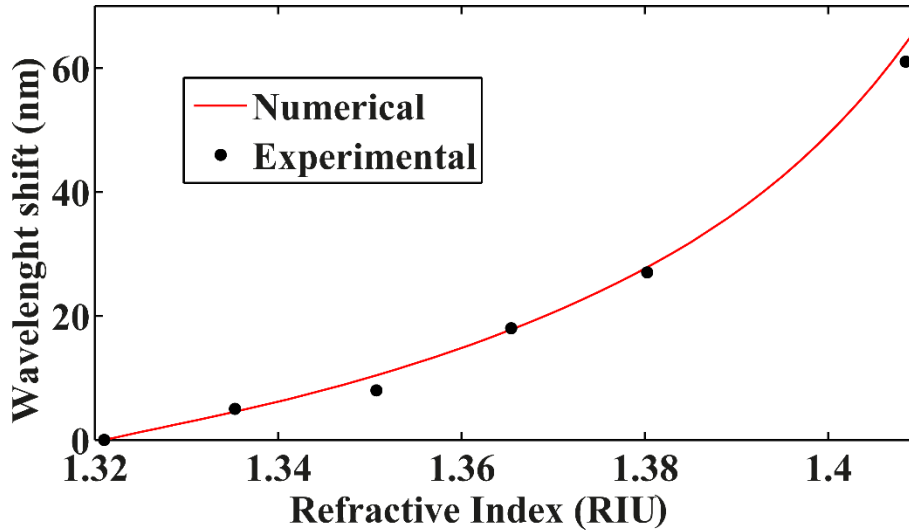


Fig. 8 Wavelength shift with refractive index experimental, and numerical for an E-SMS of 25  $\mu\text{m}$  of diameter and 14 mm of length.

## 2. Label free detection by means of wavelength and phase shift tracking

This section presents the results of the biodetection in both wavelength and phase analyses. As the role of the temperature control turned out to be essential when dealing with biosensors, a comparative analysis of the results as a function of two temperature control situations will be reported. In this approach, the results obtained with a temperature control error of  $\pm 0.5$   $^{\circ}\text{C}$  using the E-SMS 1 structure will be presented first, and later the same procedure will be presented for the E-SMS 2 structure with a temperature control error of  $\pm 0.01$   $^{\circ}\text{C}$ .

Following the protocol indicated in [6], the IgG – anti-IgG interaction was measured by increasing the anti-IgG concentration of the testing solution with rinsing stages of the biosensor using PBS solution in between. The PBS rinse stage was used to establish the baseline associated to each increasing anti-goat IgG concentration and to remove the unbound antibodies from the previous solution. Therefore, the corresponding data was collected at this stage.

Fig. 9 presents the results corresponding to bioprobe E-SMS 1 for both wavelength and phase tracking when the temperature control was  $\pm 0.5$   $^{\circ}\text{C}$ . For this purpose, the interferometric attenuation band was centered near 1376 nm, since this was the most noticeable attenuation band. Fig. 9 (a) shows the experimental wavelength tracking when the measurements increased from 2.9 mg/L to 195 mg/L, before the sensor reached saturation. In this figure, it can be seen that the total wavelength shift is 3.3 nm ranging from 1376.2 to 1379.5 nm. As mentioned before, the relevant data were collected once the response stabilized in the PBS stages. These values were plotted in Fig. 9 (b) in a logarithmic scale. A typical Hill Equation sigmoidal curve has been fitted with a correlation coefficient of 0.9981. According to this, the LOD achieved in this first experiment was 0.3 mg/L.

Simultaneously to the wavelength measurements, the phase shift was recorded in real-time. Fig. 9 (c) shows the phase shift changes when different concentrations of anti-goat IgGs were injected through the flow cell with the E-SMS 1 bioprobe. A maximum of 0.4 rad variation was registered between the mentioned increasing concentrations. Following the same procedure, a Hill Equation curve was fitted to the corresponding phase values, showing a correlation coefficient of 0.9980.

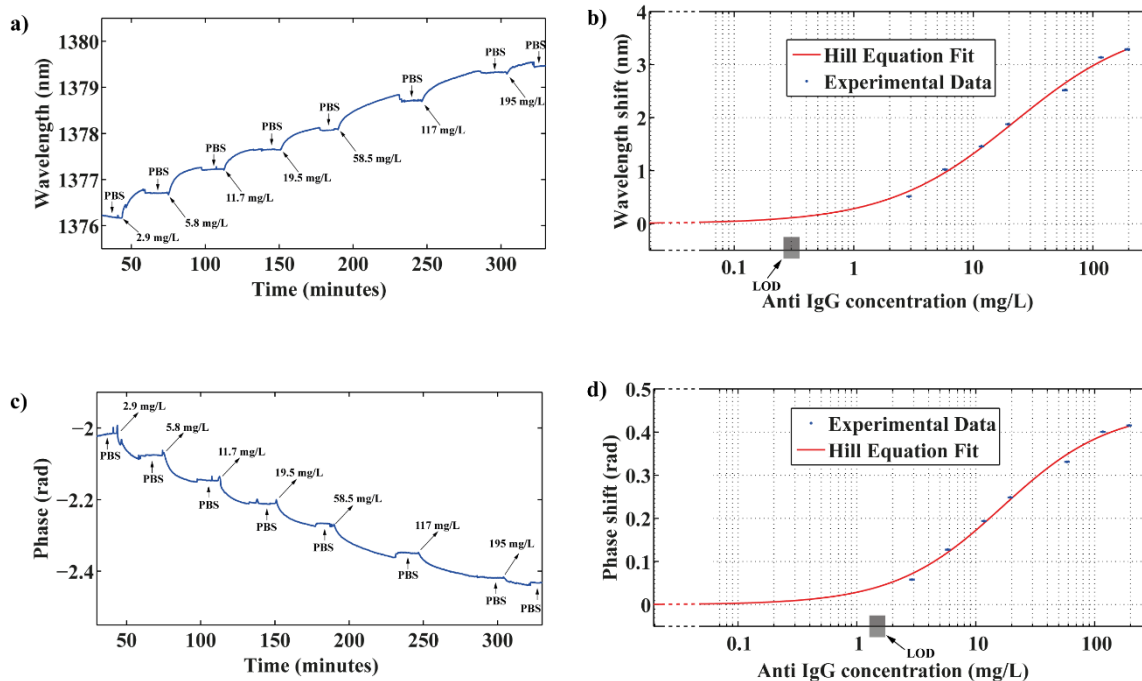


Fig. 9 Results corresponding to bioassay E-SMS 1 with different concentrations of goat anti-IgG, ranging from 2.9 mg/L to 195 mg/L. a) Wavelength response curve, b) Calibration curve in wavelength. The solid line provides the best sigmoidal curve fitting of the experimental data with a 0.9981 correlation coefficient, c) Phase response curve, d) Calibration curve of the phase shift. The solid line represents the best curve fitting for the sigmoidal Hill Equation with a 0.9980 correlation coefficient.

Then, a second bioassay using bioprobe E-SMS 2 and incorporating a better temperature control ( $\pm 0.01$  °C) was carried out. This time the concentrations to explore started in 4 mg/L, and reached 200 mg/L. In this case, the attenuation band to study was centered at 1364 nm. Once again, the results are shown in Fig. 10 both for wavelength and phase shift. The experimental wavelength tracking when the measurements increased from 4 mg/L to 200 mg/L are shown in Fig. 10 (a). Here, the total wavelength shift was in the same order than that one in the first bioassay ( $\sim 3.1$  nm). The Hill Equation fitting of Fig. 10 (b) showed a good correlation ( $R^2 = 0.9968$ ), which provided an LOD of 0.2 mg/L.

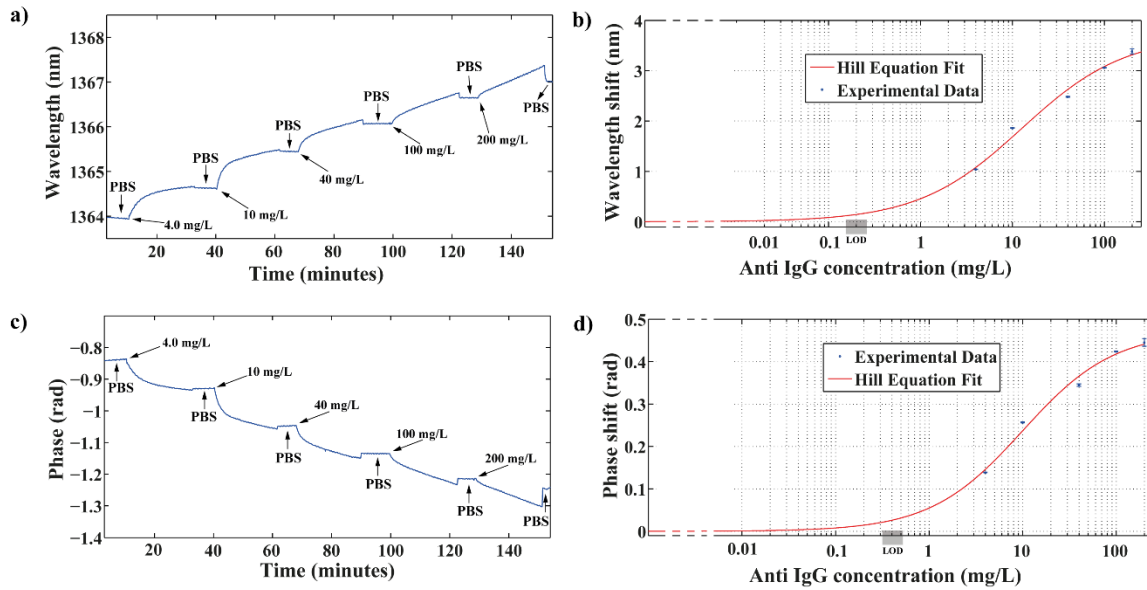


Fig. 10 Results corresponding to bioassay E-SMS 2 with different concentrations of goat anti-IgG, ranging from 4.0 mg/L to 200 mg/L using the E-SMS 2 structure, a) wavelength response curve, b) calibration curve in wavelength of the bioassay. The solid line illustrates the best sigmoidal curve fit of the experimental data with a 0.9968 correlation coefficient, c) phase response curve, d) calibration curve in phase. The solid line provides the best sigmoidal curve fitting of the experimental data with a 0.9981 correlation coefficient.

A more in-depth analysis was done by comparing the results obtained in both experiments. In this manner, Table 1 summarizes the information from the curve fitting with the Hill sigmoidal equation for both bioassays. First of all, The DSR is considered. The results of comparison of the sensors proved that the obtained DSRs are not quite different. There are some changes that are due to a not exact control of the diameter of the fiber after etching and to other factors such as the activation of the surface, the application of Eudragit, etc, but in general it can be said that the device is reproducible. Moreover, the diameter of the optical fiber could be known in view of the sensitivity of the device to refractive index, which could be used as a calibration method that is related to sensitivity to the biofilm. Also, the LOD improved in the better-controlled temperature situation ( $\pm 0.01$  °C), demonstrating the importance of a careful control of the temperature during the bioassay.

Table 1 Parameters based on Hill fitting to the two bioprobes E-SMS 1 and E-SMS 2

|   | Wavelength |         | Phase    |          |
|---|------------|---------|----------|----------|
|   | E-SMS 1    | E-SMS 2 | E-SMS 1  | E-SMS 2  |
| Correlation coefficient                                   | 0.9981     | 0.9968  | 0.9980   | 0.9981   |
| DSR   | 3.8 nm     | 3.5 nm  | 0.45 rad | 0.45 rad |
| WR (mg/L)   | 1.5-266    | 0.7-105 | 1.7-155  | 0.8-78   |
| LOD (mg/L),<br>(Chiavaioli et al.<br>recommendation [26]) | 0.3        | 0.2     | 1.5      | 0.4      |
| Lowest concentration<br>antigen used (mg/L)               | 2.9        | 4       | 2.9      | 4        |

With the results obtained after this research, it is possible to obtain LOD values as low as 0.2 mg/L by just using an E-SMS structure with the appropriate dimensions. This characteristic, along with the fact of being a cost-effective structure with considerable spectral resolution and a very stable response during the measurements, makes the E-SMS structure highly suitable for biosensing applications, especially when considering that these parameters are the key to achieve reliable measurements.

### 3. Temperature cross-sensitivity, repeatability, and selectivity

Fig. 11 shows the behavior of the wavelength shift of an attenuation band and the phase shift with the temperature setting as described in section 5 of Methods and materials. The wavelength behavior observed followed a trend imposed by the temperature's profile generated as a consequence of the set points established. The sensitivity observed was 75 pm/°C.

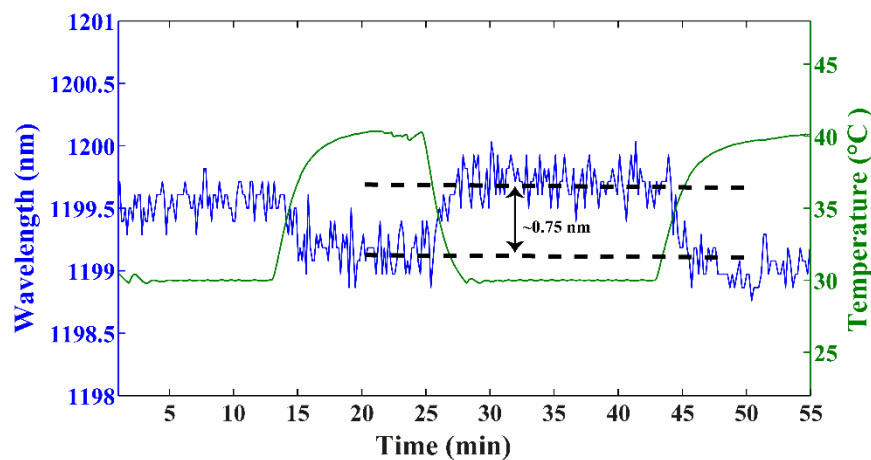


Fig. 11 Wavelength shift temperature cross sensitivity

Fig. 12 depicts the Hill equation fit with the experimental points obtained for five bioassays developed with different bioprobes fabricated by following the same procedure. Each point represents the baseline associated to each increasing anti-goat IgG concentration. Each bioassay presents the experimental points with a similar Hill fit behavior, which suggests good repeatability. In addition, the LOD found previously has been tested experimentally, in the E-SMS 5 testing a concentration of 1.0 mg/L.

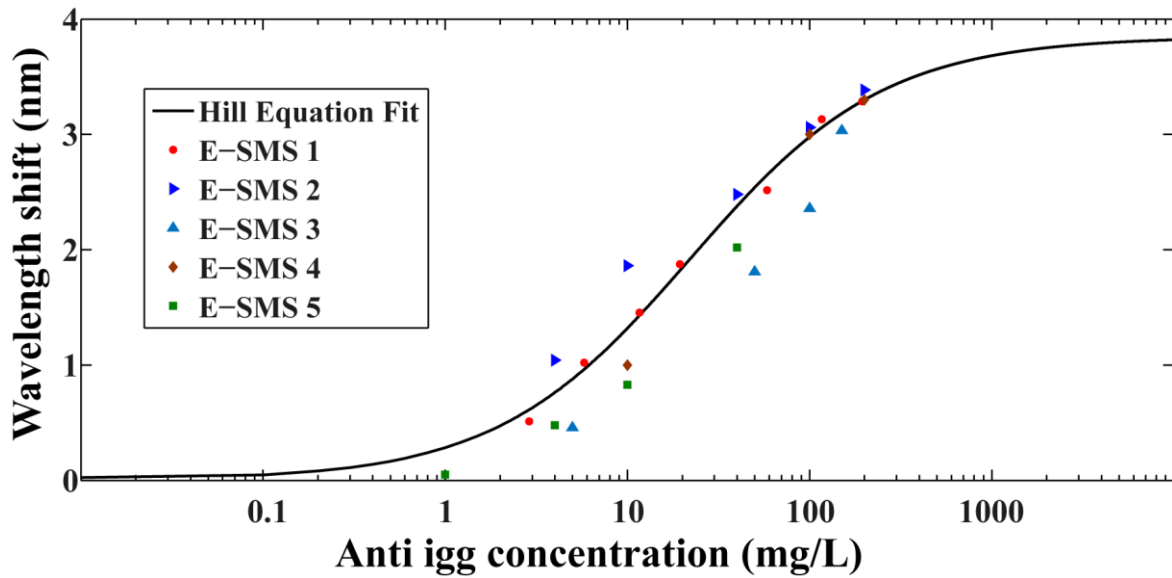


Fig. 12. Hill equation fit with the experimental points obtained for five different bioassays

The specificity test is shown in Fig. 13, where the wavelength shift was monitored in real time while different concentration of antibodies: anti-IgG and CRP were exposed to the biosensor into the flow cell system. The dotted lines indicate the moment where the antibody is exposed to the biosensor. The results show, as is well known, that IgG/anti-IgG pair has a high affinity, but, on the contrary, the CRP addition does not modify the trend followed by the previous anti-IgG addition for the E-SMS biosensor proposed in this research, which suggests a good selectivity of the target biomolecule.

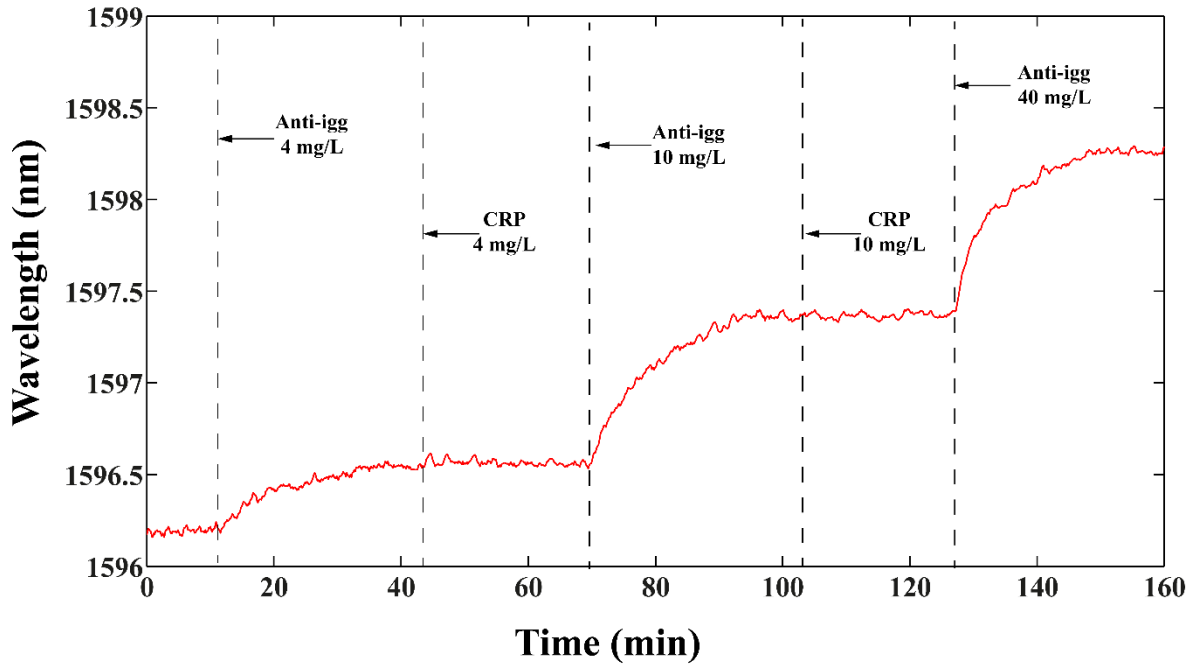


Fig. 13 Specificity test of the E-SMS biosensor

## CONCLUSIONS

The performance of E-SMS (Etched Singlemode-Multimode-Singlemode optical fiber structures) as immunosensors has been assessed by the implementation of antibody/antigen immunoassays. Through this procedure it has been proven that E-SMS structures are effective and suitable optical platforms for label-free biosensing.

In addition to the good agreement achieved between the experimental and the simulated approaches for this sensing device, it was demonstrated that the sensitivity of the SMS was enhanced by the reduction of the fiber diameter. In this research the sensitivity obtained was 280 nm/RIU in the 1.32-1.35 refractive index range when the fiber diameter was reduced until 25  $\mu\text{m}$ .

Using the phase shift and tracking the wavelength response it was found that the fabricated E-SMS exhibited a limit of detection (LOD) for solutions with a concentration of 0.2 mg/L of antibodies (anti-IgG from goat) after being coated with an antigen-based biolayer (IgG from goat).

The comparison between the LOD obtained with that one reported by others is not an easy task due to the various ways to evaluate this parameter presented in the literature. Furthermore, other factors, such as the solvent in which the target analyte was spiked, may influence the LOD determination. Despite this fact, the proposed structure could obtain LOD values comparable to those achieved by more complex structures, which places this immunosensing device as a very promising option for biological and medical applications where high sensitivities, high selectivity and compact structures are required, but with the

advantage of an inherently simpler manufacturing process. In addition, the FFT analysis technique is shown to have advantages since it could simplify the detection system making unnecessary the use of sophisticated optical interrogators.

Finally, it was noticed through the significant improvement in the LOD that measurement and proper control of the temperature of the flow cell is required to minimize errors associated to drifts induced by environmental temperature changes during long-term measurements, and to take into consideration the effects induced by pumping fluids at different temperatures within the flow channel.

### ACKNOWLEDGEMENTS

This work was supported in part by the Spanish Ministry of Education and Science-FEDER TEC 2016-78047 and by the Government of Navarre through its projects with references: 2016/PI044, 2016/PC025 and 2016/PC026.

This work was supported in part by the Colombian Administrative Department of Science, Technology and Innovation - Colciencias, through the Program for national doctorates, calling 617 of 2013, and by the project “BIOSENSORES A FIBRA ÓPTICA PARA LA DETECCIÓN RÁPIDA DE ENFERMEDADES” supported by the Universidad Nacional de Colombia (Hermes code 40834).

### REFERENCES

- [1] X. Fan, I. M. White, S. I. Shopova, H. Zhu, J. D. Suter, and Y. Sun, “Sensitive optical biosensors for unlabeled targets: A review,” *analytica chimica acta*, vol. 620, no. 1, pp. 8–26, 2008.
- [2] X. Wang and O. S. Wolfbeis, “Fiber-Optic Chemical Sensors and Biosensors (2013–2015),” *Analytical chemistry*, vol. 88, no. 1, pp. 203–227, 2015.
- [3] R. Ince and R. Narayanaswamy, “Analysis of the performance of interferometry, surface plasmon resonance and luminescence as biosensors and chemosensors,” *Analytica chimica acta*, vol. 569, no. 1, pp. 1–20, 2006.
- [4] W. E. Moerner, “New directions in single-molecule imaging and analysis,” *Proceedings of the National Academy of Sciences*, vol. 104, no. 31, pp. 12596–12602, 2007.
- [5] E. B. Shera, N. K. Seitzinger, L. M. Davis, R. A. Keller, and S. A. Soper, “Detection of single fluorescent molecules,” *Chemical Physics Letters*, vol. 174, no. 6, pp. 553–557, 1990.
- [6] F. Chiavaioli, C. Trono, A. Giannetti, M. Brenchi, and F. Baldini, “Characterisation of a label-free biosensor based on long period grating,” *Journal of biophotonics*, vol. 7, no. 5, pp. 312–322, 2014.
- [7] A. Aray, F. Chiavaioli, M. Arjmand, C. Trono, S. Tombelli, A. Giannetti, N. Cennamo, M. Soltanolkotabi, L. Zeni, and F. Baldini, “SPR-based plastic optical

- fibre biosensor for the detection of C-reactive protein in serum,” *Journal of biophotonics*, vol. 9, no. 10, pp. 1077–1084, 2016.
- [8] R. Slavík, J. Homola, J. Ctyrok, and E. Brynda, “Novel spectral fiber optic sensor based on surface plasmon resonance,” *Sensors and Actuators B: Chemical*, vol. 74, no. 1, pp. 106–111, 2001.
- [9] E. Coscelli, M. Sozzi, F. Poli, D. Passaro, A. Cucinotta, S. Selleri, R. Corradini, and R. Marchelli, “Toward a highly specific DNA biosensor: PNA-modified suspended-core photonic crystal fibers,” *IEEE Journal of Selected Topics in Quantum Electronics*, vol. 16, no. 4, pp. 967–972, 2010.
- [10] F. Chiavaioli, P. Biswas, C. Trono, S. Jana, S. Bandyopadhyay, N. Basumallick, A. Giannetti, S. Tombelli, S. Bera, A. Mallick, and others, “Sol–Gel-Based Titania–Silica Thin Film Overlay for Long Period Fiber Grating-Based Biosensors,” *Analytical chemistry*, vol. 87, no. 24, pp. 12024–12031, 2015.
- [11] Y. Zhang, H. Shibru, K. L. Cooper, and A. Wang, “Miniature fiber-optic multicavity Fabry–Perot interferometric biosensor,” *Optics letters*, vol. 30, no. 9, pp. 1021–1023, 2005.
- [12] A. Socorro, E. Santamaria, J. Fernandez-Irigoyen, I. Del Villar, J. Corres, F. Arregui, and I. Matias, “Fiber-optic immunosensor based on an etched SMS structure,” *IEEE Journal of Selected Topics in Quantum Electronics*, 2016.
- [13] Q. Wang and G. Farrell, “All-fiber multimode-interference-based refractometer sensor: proposal and design,” *Optics letters*, vol. 31, no. 3, pp. 317–319, 2006.
- [14] J. Lou, L. Tong, and Z. Ye, “Modeling of silica nanowires for optical sensing,” *Optics express*, vol. 13, no. 6, pp. 2135–2140, 2005.
- [15] A. W. Snyder and J. Love, *Optical waveguide theory*. Springer Science & Business Media, 2012.
- [16] I. D. Villar, A. B. Socorro, J. M. Corres, F. J. Arregui, and I. R. Matias, “Refractometric sensors based on multimode interference in a thin-film coated single-mode–multimode–single-mode structure with reflection configuration,” *Applied optics*, vol. 53, no. 18, pp. 3913–3919, 2014.
- [17] A. B. Socorro, E. Santamaria, J. Fernández-Irigoyen, I. Del Villar, J. M. Corres, F. J. Arregui, and I. R. Matias, “Fiber-Optic Immunosensor Based on an Etched SMS Structure,” *IEEE Journal of Selected Topics in Quantum Electronics*, vol. 23, no. 2, pp. 1–8, 2017.
- [18] I. Malitson, “Interspecimen comparison of the refractive index of fused silica\*,” *Josa*, vol. 55, no. 10, pp. 1205–1209, 1965.
- [19] Y. Cardona-Maya, I. Del Villar, A. B. Socorro, J. M. Corres, I. R. Matias, and J. F. Botero-Cadavid, “Wavelength and Phase Detection Based SMS Fiber Sensors Optimized With Etching and Nanodeposition,” *JOURNAL OF LIGHTWAVE TECHNOLOGY*, vol. 35, no. 17, p. 3743, 2017.
- [20] C. Trono, F. Baldini, M. Brenci, F. Chiavaioli, and M. Mugnaini, “Flow cell for strain-and temperature-compensated refractive index measurements by means of cascaded optical fibre long period and Bragg gratings,” *Measurement Science and Technology*, vol. 22, no. 7, p. 075204, 2011.
- [21] A. Sassolas, L. J. Blum, and B. D. Leca-Bouvier, “Immobilization strategies to develop enzymatic biosensors,” *Biotechnology advances*, vol. 30, no. 3, pp. 489–511, 2012.

- [22] R. Dudley, P. Edwards, R. Ekins, D. Finney, I. McKenzie, G. Raab, D. Rodbard, and R. Rodgers, "Guidelines for immunoassay data processing.," *Clinical chemistry*, vol. 31, no. 8, pp. 1264–1271, 1985.
- [23] M. I. Stefan and N. Le Novère, "Cooperative binding," *PLoS Comput Biol*, vol. 9, no. 6, p. e1003106, 2013.
- [24] A. V. Hill, "The possible effects of the aggregation of the molecules of haemoglobin on its dissociation curves," *J Physiol (Lond)*, vol. 40, pp. 4–7, 1910.
- [25] C. Albrecht, N. Kaepfel, and G. Gauglitz, "Two immunoassay formats for fully automated CRP detection in human serum," *Analytical and Bioanalytical Chemistry*, vol. 391, no. 5, p. 1845, 2008.
- [26] F. Chiavaioli, C. A. Gouveia, P. A. Jorge, and F. Baldini, "Towards a uniform metrological assessment of grating-based optical fiber sensors: From refractometers to biosensors," *Biosensors*, vol. 7, no. 2, p. 23, 2017.
- [27] D. Barrera, J. Villatoro, V. P. Finazzi, G. A. Cárdenas-Sevilla, V. P. Minkovich, S. Sales, and V. Pruneri, "Low-loss photonic crystal fiber interferometers for sensor networks," *Journal of Lightwave Technology*, vol. 28, no. 24, pp. 3542–3547, 2010.
- [28] D. Leandro, M. Bravo, A. Ortigosa, and M. Lopez-Amo, "Real-time FFT analysis for interferometric sensors multiplexing," *Journal of Lightwave Technology*, vol. 33, no. 2, pp. 354–360, 2015.
- [29] P. R. Cooper, "Refractive-index measurements of liquids used in conjunction with optical fibers," *Applied optics*, vol. 22, no. 19, pp. 3070–3072, 1983.
- [30] L. Hoyt, "New table of the refractive index of pure glycerol at 20 C," *Industrial & Engineering Chemistry*, vol. 26, no. 3, pp. 329–332, 1934.